

## Charge distribution and electric-field gradients in $\text{YBa}_2\text{Cu}_3\text{O}_{7-x}$

Karlheinz Schwarz, Claudia Ambrosch-Draxl, and Peter Blaha

*Institut für Technische Elektrochemie, Technische Universität Wien, A-1060 Vienna, Getreidemarkt 9/158, Austria*

(Received 28 February 1990)

The electric-field gradients (EFG's) of  $\text{YBa}_2\text{Cu}_3\text{O}_7$ ,  $\text{YBa}_2\text{Cu}_3\text{O}_{6.5}$ , and  $\text{YBa}_2\text{Cu}_3\text{O}_6$  are calculated on a first-principles basis using the full-potential linear augmented-plane-wave (LAPW) method in which exchange and correlation effects are treated by the local-density approximation (LDA). Good agreement with experimental EFG's and their anisotropies is found for the Cu(1) position in all three compounds. For  $\text{YBa}_2\text{Cu}_3\text{O}_7$ , the same is true for all oxygen positions, while at Cu(2) the direction of the EFG is predicted correctly, but a transfer of 0.07 electrons from  $d_{x^2-y^2}$  to  $d_{z^2}$  symmetry would be needed to bring the theoretical EFG into agreement with the experimental value. The EFG calculations on  $\text{YBa}_2\text{Cu}_3\text{O}_6$  and  $\text{YBa}_2\text{Cu}_3\text{O}_{6.5}$  [assuming an ordered structure in which Cu(1) is threefold coordinated by oxygens] confirm the experimental assignment and strengthen the confidence in our results. The origin of the EFG is discussed and the relation to the anisotropy of the electronic charge distribution is illustrated in connection with symmetry-decomposed partial charges and difference-electron-density maps. It is shown that the LDA calculations yield reliable charge distributions to which the EFG is so sensitive.

### I. INTRODUCTION

$\text{YBa}_2\text{Cu}_3\text{O}_7$  is one of the most prominent members of the new class of ceramic high-temperature superconductors. There is strong evidence that superconductivity occurs mainly in the  $\text{CuO}_2$  layers, while the Cu-O chains with varying oxygen content control the charge transfer into this plane. When too many oxygen defects are present, superconductivity is lost and the compound becomes antiferromagnetic and insulating. Another crucial quantity is the hole concentration which depends on the filling of certain Cu  $3d$  and O  $2p$  states. Before one can investigate the electron dynamics on a small energy scale appropriate for a fundamental understanding of superconductivity, it is important to know where the holes are and how the charge is distributed between Cu and O.

The electric-field gradient (EFG) is a ground-state property of a solid and depends sensitively on the asymmetry of the electronic charge in a crystal. In such complex materials a detailed charge distribution cannot be obtained from x-ray diffraction data, however, the EFG is ideally suited for that purpose. Experimentally, the superconductor  $\text{YBa}_2\text{Cu}_3\text{O}_7$  and the insulator  $\text{YBa}_2\text{Cu}_3\text{O}_6$  have been investigated by nuclear magnetic resonance (NMR) and nuclear quadrupole resonance (NQR) spectroscopy.<sup>1-4</sup> For  $\text{YBa}_2\text{Cu}_3\text{O}_7$ , all the NQR measurements agree in the position of the two resonance lines which were observed at 22 and 31.5 MHz. In early 1988 the assignment of these two lines to the two Cu positions was a controversial issue. At that time, no theoretical explanation was available, which could have helped to clarify the interpretation. Additional experiments on single crystals<sup>5</sup> lead to the generally agreed assignment,<sup>6</sup> that the 22-MHz resonance originates from the Cu(1) position (in the chains) and the other from Cu(2) in the plane, thus the principal components of the EFG for both Cu posi-

tions in  $\text{YBa}_2\text{Cu}_3\text{O}_7$  were known. Lütgemeier<sup>4</sup> presented NMR and NQR data for samples of varying oxygen composition. Recently,  $^{17}\text{O}$  NMR data became available, first only for some oxygen positions,<sup>7</sup> but then the EFG's and their asymmetry at all four oxygen positions were derived.<sup>8,9</sup>

The electronic structure of these systems has been obtained by various band-structure calculations (reviewed by Pickett<sup>10</sup>), which are based on the density-functional theory (DFT) in combination with the local-density approximation (LDA). Since the results of such calculations showed discrepancies to experimental spectra, and failed to reproduce the insulating and antiferromagnetic ground state in  $\text{YBa}_2\text{Cu}_3\text{O}_6$ , it has been argued that LDA calculations are not able to describe these systems. Therefore, it is important to investigate to which extent one can rely on LDA band structures. The study of EFG's for such compounds is particularly important, because EFG's depend sensitively on the charge distribution and thus provide information on the *ground state*, the only result which is given rigorously by DFT calculations. Many spectroscopies involve *excited states* and, consequently, any attempt to understand spectra on the basis of ground-state calculations relies on the assumption (which holds at best approximately), that energy eigenvalues can be interpreted as excitation energies.

In 1985 Blaha *et al.*<sup>11</sup> developed a first-principles method to compute EFG's from an all electron band-structure calculation. They have used the full-potential linear augmented-plane-wave (LAPW) method and have calculated the EFG directly from the self-consistent charge density by solving Poisson's equation without further approximations such as the use of Sternheimer antishielding factors. This method was successfully applied to the superionic conductor  $\text{Li}_3\text{N}$ ,<sup>11</sup> to all hcp metals up to Cd,<sup>12,13</sup> and to  $\text{Cu}_2\text{O}$  (cuprite).<sup>14</sup> In all these cases the

new method can explain the origin of the EFG both qualitatively and quantitatively, so that the study of the new class of ceramic superconductors is well founded.

Previously, we have performed such calculations for  $\text{YBa}_2\text{Cu}_3\text{O}_6$  and  $\text{YBa}_2\text{Cu}_3\text{O}_7$  in order to study the EFG's and have published first results in two short papers.<sup>15,16</sup> Recently, we became aware of a work by Park,<sup>17</sup> who did LAPW calculations for these two compounds and computed the EFG's by the method of Blaha *et al.*<sup>11</sup> His results differ significantly from ours, probably due to a coarser  $k$  mesh and smaller matrix size used. In the present paper we include new calculations on  $\text{YBa}_2\text{Cu}_3\text{O}_{6.5}$  and provide a detailed analysis of the various EFG contributions and relate them to anisotropies in the charge densities. From a fundamental point of view we use EFG's as sensitive quantities in order to check the validity of the LDA.

## II. STRUCTURES

$\text{YBa}_2\text{Cu}_3\text{O}_{7-x}$  varies from a superconducting phase for  $x=0$  ( $\text{YBa}_2\text{Cu}_3\text{O}_7$ ) to an antiferromagnetic insulator for  $x=1$  ( $\text{YBa}_2\text{Cu}_3\text{O}_6$ ). Removing all O(1) atoms from the  $\text{YBa}_2\text{Cu}_3\text{O}_7$  structure (Fig. 1) leads to the tetragonal  $\text{YBa}_2\text{Cu}_3\text{O}_6$ . Near  $x=0.5$  superconductivity disappears and there are several ways in which the oxygen defects can be arranged. The most stable structure of  $\text{YBa}_2\text{Cu}_3\text{O}_{6.5}$  turns out to be the double-cell phase<sup>18,19</sup> with parallel Cu-O chains running through every second Cu(1) (as in  $\text{YBa}_2\text{Cu}_3\text{O}_7$ ) while the chain in between has lost all the O(1) atoms as in  $\text{YBa}_2\text{Cu}_3\text{O}_6$ . These two types of copper atoms have coordination numbers of four and two, respectively. Since there is also evidence for threefold coordination,<sup>4,20</sup> we try to simulate this situation by assuming another arrangement in which the O(1) atoms and oxygen vacancies alternate in every Cu(1)-O(1) chain and neighboring chains are shifted by one lattice spacing as shown in Fig. 2; here both the  $a$  and  $b$  parameters are

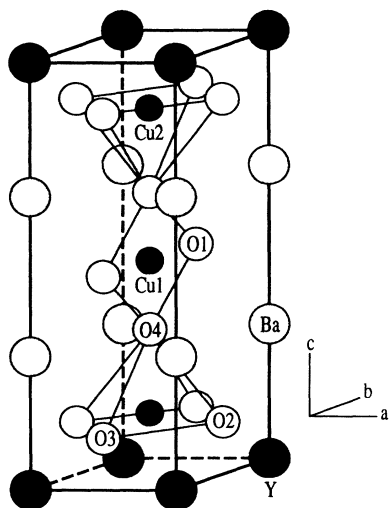


FIG. 1. Unit cell of  $\text{YBa}_2\text{Cu}_3\text{O}_7$  with standard labeling of the atoms.

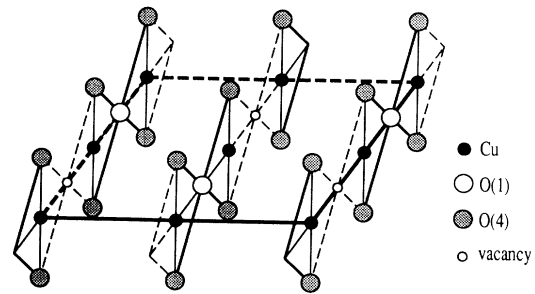


FIG. 2. In  $\text{YBa}_2\text{Cu}_3\text{O}_{6.5}$ , half of the O(1) atoms (see Fig. 1) are missing. Here an ordered defect structure is assumed in which Cu(1) is threefold coordinated and the oxygen vacancies alternate in neighboring Cu(1)-O(1) chains in a certain pattern. In addition, the O(4) atoms above and below the Cu(1)-O(1) plane are shown. The other atoms [Cu(2), O(2), O(3), Y, and Ba] have the corresponding positions as in  $\text{YBa}_2\text{Cu}_3\text{O}_7$  (see Sec. II).

doubled with respect to  $\text{YBa}_2\text{Cu}_3\text{O}_6$ . The oxygen position O(3) is split into the two new positions O(3) and O(3'), where the former has an O(1) neighbor and the latter an oxygen vacancy along the  $c$  direction.

$\text{YBa}_2\text{Cu}_3\text{O}_7$  and  $\text{YBa}_2\text{Cu}_3\text{O}_{6.5}$  (as in Fig. 2) are orthorhombic with space groups  $Pmmm$  and  $Cmmm$ , respectively;  $\text{YBa}_2\text{Cu}_3\text{O}_6$  is tetragonal with space group  $P4/mmm$ . The structural parameters of  $\text{YBa}_2\text{Cu}_3\text{O}_7$  are taken from Beno *et al.*<sup>21</sup> and of  $\text{YBa}_2\text{Cu}_3\text{O}_6$  from Hewat *et al.*<sup>22</sup> (using the data at 100 °C). For the assumed structure of  $\text{YBa}_2\text{Cu}_3\text{O}_{6.5}$  the following lattice parameters are used:  $a=b=14.6132$  a.u.,  $c=22.4541$  a.u., and all the fractional coordinates remain identical to  $\text{YBa}_2\text{Cu}_3\text{O}_6$ .

## III. COMPUTATIONAL DETAILS

We utilize the well known full-potential LAPW method in which no shape approximation on either the potential or the electronic charge density is made and use the WIEN code.<sup>23</sup> The computational details are now summarized.

The following atomic sphere radii are used in the  $\text{YBa}_2\text{Cu}_3\text{O}_7$  calculation: 2.74, 2.9, 1.9, and 1.55 a.u. for Y, Ba, Cu, and O, respectively. In  $\text{YBa}_2\text{Cu}_3\text{O}_{6.5}$  and  $\text{YBa}_2\text{Cu}_3\text{O}_6$  the Cu(1) radius was reduced to 1.80 a.u.; a limit of 1000 plane waves for  $\text{YBa}_2\text{Cu}_3\text{O}_7$  and  $\text{YBa}_2\text{Cu}_3\text{O}_6$  and 1500 for  $\text{YBa}_2\text{Cu}_3\text{O}_{6.5}$ , and a maximum of  $l=12$  in the wave functions is used. The potential (and charge density) is expanded inside the atomic spheres in crystal harmonics up to  $L=4$  with the exception of  $\text{YBa}_2\text{Cu}_3\text{O}_{6.5}$ , where the expansion is limited by  $L=3$  inside the atomic spheres of Ba, Cu(2), O(2), and O(4). In the interstitial region a Fourier series with 999, 1147, and 674  $k$  stars is used for  $\text{YBa}_2\text{Cu}_3\text{O}_7$ ,  $\text{YBa}_2\text{Cu}_3\text{O}_{6.5}$ , and  $\text{YBa}_2\text{Cu}_3\text{O}_6$ , respectively.

The Y 4s, Y 4p, Ba 5s, and Cu 3p states lie between  $-5$  and  $-1$  Ry and their charges are not completely confined inside the respective atomic spheres (see, for example, the Cu 3p wave functions in Fig. 6). They are treated as semicore states in an additional band calculation<sup>23</sup> using 9  $k$  points in the irreducible wedge of the Brillouin zone

(IBZ). For the valence states, 50  $k$  points are used in the IBZ for  $\text{YBa}_2\text{Cu}_3\text{O}_7$ . In the tetragonal  $\text{YBa}_2\text{Cu}_3\text{O}_6$  the equivalent mesh consists of 30  $k$  points for the valence and 6 for the semicore states, while in  $\text{YBa}_2\text{Cu}_3\text{O}_{6.5}$  a mesh of 24(4)  $k$  points for the valence (semicore) states is used. All three compounds,  $\text{YBa}_2\text{Cu}_3\text{O}_7$ ,  $\text{YBa}_2\text{Cu}_3\text{O}_{6.5}$ , and  $\text{YBa}_2\text{Cu}_3\text{O}_6$  are studied by non-spin-polarized calculations, most of which were performed on an Apollo Workstation DN-10000.

#### IV. THE ELECTRIC-FIELD GRADIENT

##### A. Method of computation

All nuclei with a nuclear-spin quantum number  $I \geq 1$  have a nonspherical nuclear charge distribution and an electric quadrupole moment  $Q$ . The nuclear quadrupole (NQ) interaction between this  $Q$  and the electric-field gradient determines the NQ coupling constant  $eQV_{zz}/h$ , where  $e$  is the electric charge,  $h$  is Planck's constant, and  $V_{zz}$  represents the principal component of the EFG. The EFG is defined as the second derivative of the electrostatic potential written as a traceless tensor.<sup>24</sup> When this potential, which can be obtained directly from all the electronic and nuclear charges, is expanded in an  $LM$  representation, only  $L=2$  terms contribute to the second derivative and thus to the EFG.

The general expression for the principal component of the EFG arising from a charge density  $\rho(\mathbf{r})$  is defined as<sup>24</sup>

$$V_{zz} = \int \rho(\mathbf{r}) \frac{2P_2(\cos\vartheta)}{r^3} d\mathbf{r}, \quad (1)$$

where  $P_2$  is the second-order Legendre polynomial.

Blaha *et al.* have developed a new method for computing the EFG by a first-principles method.<sup>11-13,25</sup> This scheme is based on a full-potential LAPW calculation in which the unit cell is divided into nonoverlapping atomic spheres (with radii  $R_i$ ) and in an interstitial region: Inside the spheres the charge density (and, analogously, the potential) is written as a radial function  $\rho_{LM}(r)$  times the symmetrized spherical harmonics  $Y_{LM}(\hat{\mathbf{r}})$  (crystal harmonics) and in the interstitial region as a Fourier series:

$$\rho(r) = \begin{cases} \sum_{L,M} \rho_{LM}(r) Y_{LM}(\hat{\mathbf{r}}) & \text{inside sphere} \\ \sum_{\mathbf{K}} \rho(\mathbf{K}) e^{i\mathbf{K}\cdot\mathbf{r}} & \text{interstitial.} \end{cases} \quad (2)$$

The charge-density coefficients  $\rho_{LM}(r)$  can be obtained from the wave functions by (in a shorthand notation)

$$\rho_{LM}(r) = \sum_{E_{nk} < E_F} \sum_{l,m} \sum_{l',m'} R_{lm}(r) R_{l'm'}(r) G_{ll'}^{Mmm'}, \quad (3)$$

where  $G_{ll'}^{Mmm'}$  are Gaunt numbers and  $R_{lm}(r) = A_{lm} u_l(r) + B_{lm} \dot{u}_l(r)$  denote the LAPW radial wave functions (of state  $E_{nk}$ ) in the standard notation.<sup>25</sup>

For a given charge density, the Coulomb potential is obtained numerically by solving Poisson's equation in the form of a boundary value problem using a method proposed by Weinert.<sup>26</sup> This yields the potential coefficients

$\rho_{LM}(r)$  analogous to Eq. (2). For the EFG calculation, only the  $L=2$  terms near the nucleus are needed; in the limit  $r \rightarrow 0$  the asymptotic form of the potential  $r^L V_{LM} Y_{LM}$  can be used and this procedure yields

$$\begin{aligned} V_{2M} = & -C_{2M} \int_0^R \rho_{2M}(r)/r dr \\ & + C_{2M} \int_0^R \rho_{2M}(r)(r/R)^5/r dr \\ & + 5C_{2M}/R^2 \sum_K V(K) j_2(KR) Y_{2M}(K) \end{aligned} \quad (4)$$

with  $C_{20} = 2(4\pi/5)^{1/2}$ ,  $C_{22} = (3/4)^{1/2} C_{20}$ , and the spherical Bessel function  $j_2$ . In Eq. (4) we use signs opposite to a previous publication<sup>25</sup> in order to match the experimental sign convention for the electron density. The first term (called *valence* EFG) corresponds to the integral of Eq. (1), but taken only over the atomic sphere, where integration over  $\vartheta$  and  $\varphi$  changes the factor from  $1/r^3$  in Eq. (1) to  $1/r$  in the radial integral. The second and third terms (called *lattice* EFG) arise from the boundary value problem and from charge contributions outside the considered sphere. With these definitions the diagonal terms of the traceless EFG tensor with respect to the crystallographic axis  $a$ ,  $b$ , and  $c$  are

$$\begin{aligned} V_{aa} &= -\frac{1}{2} V_{20} + V_{22}, \\ V_{bb} &= -\frac{1}{2} V_{20} - V_{22}, \\ V_{cc} &= V_{20}. \end{aligned} \quad (5)$$

In most of the present cases the off-diagonal elements of the EFG tensor vanish due to symmetry, but in  $\text{YBa}_2\text{Cu}_3\text{O}_{6.5}$  nondiagonal  $V_{ab}$  terms exist for Ba, Cu(2), O(2), and O(4) and thus require diagonalization of the EFG tensor. By ordering the components (in the simple case  $V_{aa}$ ,  $V_{bb}$ , and  $V_{cc}$ ) according to their magnitudes we define

$$|V_{zz}| \geq |V_{yy}| \geq |V_{xx}|. \quad (6)$$

The EFG tensor is characterized by the largest component  $V_{zz}$  (in short EFG) and the anisotropy parameter  $\eta$  is defined as

$$\eta = (V_{xx} - V_{yy})/V_{zz}, \quad (7)$$

where  $\eta$  varies between 0 (axial symmetry) and 1 ( $V_{xx} = 0$ ).

##### B. Results

Band structures and densities of states of  $\text{YBa}_2\text{Cu}_3\text{O}_6$  and  $\text{YBa}_2\text{Cu}_3\text{O}_7$  have been published several times,<sup>10</sup> thus there is no need to show them again. Small differences between the results of various groups exist<sup>10,27,28</sup> with ours being in the same range. In a system as complicated as  $\text{YBa}_2\text{Cu}_3\text{O}_7$  it is difficult to reach convergence in the band calculations which can be regarded as the LDA limit. The accuracy of our LAPW results depends on the number of  $k$  points in the BZ, on the  $LM$  combinations and Fourier coefficients in the expansion of the potential and charge density, and on the number of plane waves in

TABLE I. Theoretical and experimental electric-field gradients (in  $10^{21} \text{ V m}^{-2}$ ) and asymmetry parameters for  $\text{YBa}_2\text{Cu}_3\text{O}_7$ ,  $\text{YBa}_2\text{Cu}_3\text{O}_{6.5}$ , and  $\text{YBa}_2\text{Cu}_3\text{O}_6$ . The sign of the EFG is not known experimentally. The experimental data on copper in  $\text{YBa}_2\text{Cu}_3\text{O}_7$  are taken from Pennington *et al.* (Ref. 5) and for oxygen from Takigawa *et al.* (Ref. 8). The Cu(1) values in  $\text{YBa}_2\text{Cu}_3\text{O}_{6.5}$  and  $\text{YBa}_2\text{Cu}_3\text{O}_6$  are from Lütgemeier (Ref. 4) and the Cu(2) data in  $\text{YBa}_2\text{Cu}_3\text{O}_6$  from Yasuoka *et al.* (Ref. 34).

		$\text{YBa}_2\text{Cu}_3\text{O}_7$		$\text{YBa}_2\text{Cu}_3\text{O}_{6.5}$		$\text{YBa}_2\text{Cu}_3\text{O}_6$	
		Theory	Expt.	Theory	Expt.	Theory	Expt.
Y	EFG	3.4		3.8		3.6	
	$\eta$	0.9		0.0		0.0	
Ba	EFG	7.3		8.0		11.0	
	$\eta$	0.8		0.3		0.0	
Cu(1)	EFG	7.4	7.5	-9.5	8.4	-10.9	11.8
	$\eta$	0.8	1.0	0.9	1.0	0.0	0.0
Cu(2)	EFG	-5.6	12.3	-2.9		-3.6	9.0
	$\eta$	0.1	0.0	0.1		0.0	0.0
O(1)	EFG	18.3	17.3	23.3			
	$\eta$	0.3	0.4	0.2			
O(2)	EFG	11.8	10.5	11.3		10.7	
	$\eta$	0.2	0.2	0.2		0.2	
O(3)	EFG	11.9	10.2	11.4		10.7	
	$\eta$	0.2	0.2	0.2		0.2	
O(3')	EFG	11.9	10.2	11.3		10.7	
	$\eta$	0.2	0.2	0.2		0.2	
O(4)	EFG	11.7	11.6	7.8		6.7	
	$\eta$	0.2	0.3	0.2		0.0	

the LAPW basis. We have increased all these limits to the values specified in Sec. III and found good convergence. Thus we are sufficiently confident that our EFG results are reliable to about 10% and the asymmetry parameter to about 0.1, so that we are able to test the validity of the present form of the LDA.

In Table I our calculated EFG's and their asymmetry parameters  $\eta$  are compared with available experimental data. In the conversion from NQR frequencies to EFG's, we use the recent nuclear quadrupole moment  $Q = -0.211b$  for  $^{63}\text{Cu}$  by Sternheimer<sup>29</sup> and the usual value<sup>30</sup>  $Q = -0.026b$  for  $^{17}\text{O}$ . The Y values cannot be measured, since there is no isotope with a nuclear quadrupole moment, and we are not aware of any Ba data.

(See note added in proof.) Most experiments obtained only the magnitude of the EFG and the asymmetry parameter,<sup>1,3,4,6</sup> however, for  $\text{YBa}_2\text{Cu}_3\text{O}_7$ , Pennington *et al.*<sup>5</sup> have measured on single crystals and thus could also determine the orientation of the EFG's. Good agreement is found between our first-principles calculations and the experimental values for all copper and oxygen positions except for Cu(2), where theory predicts only half the experimental value. An analysis of this situation will be given in Sec. VI. The EFG components for  $\text{YBa}_2\text{Cu}_3\text{O}_7$  are shown in Table II and are compared to single-crystal data<sup>5</sup> and aligned powder data.<sup>8</sup> Note that the orientation of the EFG tensor agrees for all positions.

TABLE II. Electric-field-gradient components (in  $10^{21} \text{ V m}^{-2}$ ) for  $\text{YBa}_2\text{Cu}_3\text{O}_7$ . The experimental data for copper are taken from Pennington *et al.* (Ref. 5) and for the oxygen from Takigawa *et al.* (Ref. 8).

Position		$V_{aa}$	$V_{bb}$	$V_{cc}$	$\eta$
Y	Theory	-0.2	-3.2	3.4	0.9
	Ba	Theory	-6.7	-0.6	7.3
Cu(1)	Theory	-6.7	7.4	-0.7	0.8
	Expt.	$\mp 7.4$	$\pm 7.5$	$\pm 0.0$	1.0
Cu(2)	Theory	3.0	2.6	-5.6	0.1
	Expt.	$\pm 6.2$	$\pm 6.2$	$\mp 12.3$	0.0
O(1)	Theory	-6.1	18.3	-12.2	0.3
	Expt.	$\mp 5.1$	$\pm 17.3$	$\mp 12.1$	0.4
O(2)	Theory	11.8	-7.0	-4.8	0.2
	Expt.	$\pm 10.5$	$\mp 6.3$	$\mp 4.1$	0.2
O(3)	Theory	-7.0	11.9	-4.9	0.2
	Expt.	$\mp 6.3$	$\pm 10.2$	$\mp 3.9$	0.2
O(4)	Theory	-4.7	-7.0	11.7	0.2
	Expt.	$\mp 4.0$	$\mp 7.6$	$\pm 11.6$	0.3

## V. CHARGE DISTRIBUTION

The EFG is rather sensitive to the charge distribution and thus small changes or differences could have significant effects. In the LAPW formalism the electronic charge inside one unit cell falls either in the interstitial region or in one of the atomic spheres in which a symmetry decomposition according to  $lm$  can be made. Note that this partitioning causes these values to depend on the choice of sphere radii (specified in Sec. III). Such partial charges are summarized for the valence states in Table III and for the semicore states in Table IV. Since the charge in the interstitial region is represented as a Fourier series [according to Eq. (1)] it cannot be separated into atomic or angular-projected contributions.

## A. Valence states

The following atomic notation characterizes the valence states of the constituent atoms in the  $\text{YBa}_2\text{Cu}_3\text{O}_x$  systems: Y ( $5s, 5p, 4d$ ), Ba ( $6s, 5p, 5d$ ), Cu ( $4s, 4p, 3d$ ), and O ( $2s, 2p$ ). The corresponding partial charges are given in Table III and show that Y and Ba have certainly lost some of their valence electrons, although one should keep in mind that—especially for  $s$  and  $p$  states—a large fraction of the charge lies outside the atomic sphere. Since in

$\text{YBa}_2\text{Cu}_3\text{O}_7$  the same radius is used for both copper spheres, a direct comparison between the two copper sites is meaningful and yields a smaller charge for Cu(1) with respect to Cu(2) [in  $\text{YBa}_2\text{Cu}_3\text{O}_{6.5}$  and  $\text{YBa}_2\text{Cu}_3\text{O}_6$  the Cu(1) radius is 1.8 a.u., while it is 1.9 a.u. for Cu(2)].

For the Cu  $3d$  charges, which are dominated by the Cu on-site component (i.e., a  $3d$  wave function centered on copper), a simple frontier orbital picture is useful. Cu has an almost filled  $d$  shell and thus interaction with oxygen leads to bonding and antibonding orbitals most of which are essentially filled. If they are not completely occupied, it is the antibonding part which remains empty and this situation leads to smaller charges and favors shorter distances, e.g., for Cu(1) and O(4). For both, Cu(1) and Cu(2), the  $d_{z^2}$  and the  $d_{x^2-y^2}$  states are not completely filled and therefore their charge is smaller than that of the other three  $d$  symmetries, namely  $d_{xy}$ ,  $d_{xz}$ , and  $d_{yz}$  which are nearly filled leading to a charge of about  $1.86e$  inside the copper sphere. For Cu(2) there is more charge in the  $d_{z^2}$  orbital than in  $d_{x^2-y^2}$  since the former has weak interactions with  $p$  orbitals on O(4) leading to narrow bands which are almost filled. The latter interacts strongly with  $p$  orbitals on O(2) and O(3), yielding broad bands whose antibonding part is partly unoccupied and, therefore, the distances to O(2) and O(3) are shorter than

TABLE III. Partial charges (in electrons) of the valence states and their symmetry decomposition, where the Cartesian coordinates are assumed to be parallel to the crystallographic axes:  $x||a, y||b, z||c$ . In  $\text{YBa}_2\text{Cu}_3\text{O}_6$  the O(2) and O(3) positions are crystallographically equivalent but differ in their orientation with respect to  $x$  and  $y$ .

	$s$	$p$	$d$	$f$	$p_x$	$p_y$	$p_z$	$d_{x^2}$	$d_{x^2-y^2}$	$d_{xy}$	$d_{xz}$	$d_{yz}$
<b><math>\text{YBa}_2\text{Cu}_3\text{O}_7</math></b>												
Y	0.18	0.26	0.87	0.13	0.09	0.08	0.09	0.09	0.23	0.08	0.25	0.22
Ba	0.06	5.57	0.29	0.07	1.86	1.86	1.85	0.06	0.04	0.09	0.06	0.04
Cu(1)	0.23	0.20	8.60	0.02	0.03	0.07	0.10	1.41	1.65	1.84	1.84	1.86
Cu(2)	0.20	0.17	8.69	0.02	0.07	0.07	0.03	1.76	1.44	1.85	1.82	1.82
O(1)	1.55	3.34	0.01	0.00	1.18	0.91	1.25					
O(2)	1.54	3.40	0.01	0.00	1.01	1.21	1.18					
O(3)	1.54	3.39	0.01	0.00	1.21	1.00	1.18					
O(4)	1.54	3.36	0.01	0.00	1.18	1.19	0.99					
<b><math>\text{YBa}_2\text{Cu}_3\text{O}_{6.5}</math></b>												
Y	0.17	0.25	0.83	0.12	0.08	0.08	0.09	0.08	0.22	0.07	0.23	0.23
Ba	0.05	5.56	0.26	0.06	1.86	1.86	1.84	0.05	0.03	0.09	0.05	0.04
Cu(1)	0.21	0.15	8.51	0.01	0.02	0.04	0.09	1.47	1.68	1.77	1.79	1.80
Cu(2)	0.20	0.17	8.70	0.01	0.07	0.07	0.03	1.77	1.47	1.84	1.81	1.81
O(1)	1.57	3.25	0.01	0.00	1.18	0.80	1.27					
O(2)	1.54	3.36	0.01	0.00	1.00	1.19	1.17					
O(3)	1.54	3.37	0.01	0.00	1.20	1.00	1.17					
O(3')	1.54	3.36	0.01	0.00	1.19	1.00	1.17					
O(4)	1.55	3.34	0.01	0.00	1.16	1.15	1.03					
<b><math>\text{YBa}_2\text{Cu}_3\text{O}_6</math></b>												
Y	0.17	0.25	0.87	0.13	0.08	0.08	0.09	0.09	0.22	0.08	0.24	0.24
Ba	0.06	5.56	0.28	0.07	1.86	1.86	1.84	0.05	0.04	0.09	0.05	0.05
Cu(1)	0.22	0.13	8.58	0.01	0.02	0.02	0.09	1.48	1.75	1.75	1.80	1.80
Cu(2)	0.20	0.17	8.71	0.02	0.07	0.07	0.03	1.77	1.46	1.84	1.82	1.82
O(2)	1.54	3.37	0.01	0.00	1.01	1.19	1.17					
O(3)	1.54	3.37	0.01	0.00	1.19	1.01	1.17					
O(4)	1.54	3.36	0.01	0.00	1.15	1.15	1.06					

TABLE IV. Partial charges (in electrons) of the Y 4s and Y 4p, Ba 5s, and Cu 3p semicore states (for orientation see Table III).

	<i>s</i>	<i>p</i>	<i>p<sub>x</sub></i>	<i>p<sub>y</sub></i>	<i>p<sub>z</sub></i>
YBa <sub>2</sub> Cu <sub>3</sub> O <sub>7</sub>					
Y	1.99	5.58	1.859	1.869	1.852
Ba	1.93	0.00	0.000	0.000	0.000
Cu(1)	0.00	5.97	1.991	1.991	1.991
Cu(2)	0.00	5.97	1.991	1.991	1.991
YBa <sub>2</sub> Cu <sub>3</sub> O <sub>6.5</sub>					
Y	1.99	5.58	1.864	1.864	1.850
Ba	1.94	0.00	0.000	0.000	0.000
Cu(1)	0.00	5.95	1.984	1.984	1.983
Cu(2)	0.00	5.97	1.990	1.990	1.990
YBa <sub>2</sub> Cu <sub>3</sub> O <sub>6</sub>					
Y	1.99	5.60	1.869	1.869	1.856
Ba	1.94	0.00	0.000	0.000	0.000
Cu(1)	0.00	5.95	1.985	1.985	1.984
Cu(2)	0.00	5.97	1.991	1.991	1.991

to O(4) and the  $d_{x^2-y^2}$  charge is smaller than that of  $d_{z^2}$ .

For YBa<sub>2</sub>Cu<sub>3</sub>O<sub>7</sub> (YBa<sub>2</sub>Cu<sub>3</sub>O<sub>6.5</sub>) an analysis of the partial charges on Cu(1) is better carried out in a different coordinate system in which the *x* and *z* axis are interchanged, i.e.,  $z \parallel a$ . With this choice of coordinates the occupation of the  $d_{z^2}$  orbital is 1.74 (1.70)*e* and is large as a consequence of weak interactions, however, that of  $d_{x^2-y^2}$  is small, namely 1.32 (1.45)*e* (different than in Table III which refers to the standard coordinate system). The latter value is small, since the antibonding part of the broad band arising from strong interactions remains unoccupied leading to short Cu(1)-O(4) distances.

For the oxygen sites, the symmetry-decomposed *p*-like partial charges show the most interesting effects: two of the partial charges are around 1.2*e*, while the third one is around 1.0*e*. For the O(2) sphere (the one labeled in Fig. 1), for example, the  $p_y$  and  $p_z$  orbitals are involved in weak interactions and thus their bands are narrow and mostly occupied (with charges around 1.2*e*), while the  $p_x$  orbital has a strong interaction with the Cu(2)  $d_{x^2-y^2}$  orbital and the Fermi energy falls in the antibonding part of that band leading to only partial occupation (with a charge around 1.0*e*). An analogous situation occurs for O(3) only that *x* and *y* are interchanged. Similarly, the strong interactions of Cu(1) with O(1) and O(4) lead to smaller occupation numbers in the corresponding symmetries, where the  $p_y$  charge on O(1) is the smallest of all oxygen *p*-like charges.

The charges corresponding to the Cu-4*p* states are relatively small, but they play an important role in the understanding of the EFG. The Cu-4*p* are not "real" (on-site) Cu-4*p* states, which lie at much higher energies, but represent the partial wave expansion inside the copper sphere (Fig. 6) of wave functions centered on neighboring sites (off site). They originate mainly from the surrounding oxygen 2*p* wave functions and their respective charges correlate with the distances to the oxygen neighbors (Fig. 1) but in the opposite direction to the (on site)

Cu *d* components discussed earlier. In YBa<sub>2</sub>Cu<sub>3</sub>O<sub>7</sub> the distance Cu(1)-O(4) is smaller than Cu(1)-O(1), thus the charge of 4*p<sub>z</sub>* is larger than that of 4*p<sub>y</sub>*; the smallest component is 4*p<sub>x</sub>*, since the oxygen neighbors are missing in the *a* direction. In YBa<sub>2</sub>Cu<sub>3</sub>O<sub>6</sub>, where no O(1) sites are present, the charges for 4*p<sub>y</sub>* and 4*p<sub>x</sub>* are small and must be equal due to the tetragonal symmetry.

### B. Semicore states

The charge of semicore states is (by definition) not completely confined inside the respective atomic sphere in contrast to true core states. Therefore, we have treated them as bandlike states in a separate band calculation using a different energy window. This procedure is routinely used in many of our calculations,<sup>23</sup> but when the EFG's are studied, it is important to allow for core polarization, since small anisotropies in the semicore charge distribution could have significant effects. Sorantin<sup>31</sup> was the first, who found such a situation when he studied TiO<sub>2</sub> in the rutile structure.

The partial charges of the semicore states are presented in Table IV, where the small charges inside the oxygen spheres are omitted. The latter originate from the tails of the wave functions of the neighboring atoms. Since for O(1) and O(4) less than 0.001*e* is found inside their spheres, the semicore states of neither Cu nor Ba contribute, although they are neighbors (Fig. 1). For O(2) and O(3), however, an *s*-like charge of 0.04*e*, 0.002*e* of  $p_z$  and 0.003*e* of  $p_x$  or  $p_y$  symmetry is found for all three compounds. Since these values depend only on the orientation where the next Y atoms are, these charges originate from the tails of the Y-4*p* states. This observation is consistent with *p*-like partial charges on Y which are different for *x*, *y*, and *z*, while they agree to within 0.001*e* for copper. Whenever a semicore charge extends into the neighboring sphere, it is likely that polarization effects play a role for the central atom.

### C. Electron densities

The charge distribution of  $\text{YBa}_2\text{Cu}_3\text{O}_7$  as obtained in the present LAPW calculation is shown in Fig. 3 as difference electron density  $\Delta\rho$  in the  $yz$  plane, i.e.,  $\parallel b$  and  $\parallel c$  (see Fig. 1).  $\Delta\rho$  is taken between the (LAPW) crystalline and the superposed ionic densities of the free ions  $\text{Y}^{3+}$ ,  $\text{Ba}^{2+}$ ,  $\text{Cu}^+$  (with  $3d^{10}$ ), and oxygen with an ionicity of  $-\frac{10}{7}$  (in order to keep electroneutrality). When another set of ionicities (e.g., a combination with  $\text{Cu}^{2+}$  and  $\text{O}^{2-}$ ) is used, details change but the overall picture in the form of the anisotropies remains. As mentioned before,<sup>28</sup> the antibonding band, involving  $\text{Cu}(2) d_{x^2-y^2}$  and  $\text{O}(3) p_y$  orbitals in the  $\text{CuO}_2$  plane, is only partly occupied (Table III). This can be clearly seen from  $\Delta\rho$  shown in Fig. 3 (showing a section perpendicular to this plane), where the corresponding states show up as negative contour lines along the  $b$  axis. The hole states have been investigated by several spectroscopies which try to analyze their character and symmetry.<sup>32,33</sup> We clearly do not find “out-of-plane  $\pi$  holes” in agreement with electron-energy-loss spectra,<sup>33</sup> but we can also rule out “in-plane  $\pi$  holes,” a result which is not evident from  $\Delta\rho$  in the  $yz$  plane (Fig. 3) but follows from the corresponding partial charges (Table III). While experiment<sup>33</sup> cannot distinguish between “in-plane  $\sigma$ ” and “in-plane  $\pi$ ” holes, our calculation yields the former. Anisotropies in the charge distribution occur for all copper and oxygen atoms near the

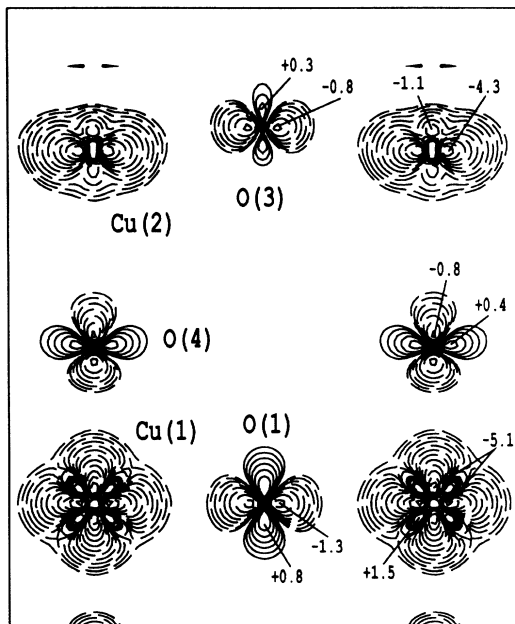


FIG. 3. Difference electron density taken between the crystalline (LAPW) and the superposed ionic densities assuming the ions  $\text{Y}^{3+}$ ,  $\text{Ba}^{2+}$ ,  $\text{Cu}^{1+}$ , and  $\text{O}^{10/7-}$ . A contour plot is shown in a plane parallel to the  $b$  and  $c$  axis through the  $\text{Cu}(1)\text{--O}(1)$  chains cutting the atoms  $\text{O}(4)$ ,  $\text{Cu}(2)$ , and  $\text{O}(3)$  (see Fig. 1), maxima and minima are labeled in units of  $e/\text{\AA}^3$ ; contour lines start with  $\pm 0.1$  and differ by a factor  $\sqrt{2}$  for positive (solid) and negative (dashed) values.

respective nucleus and originate from the (often antibonding) bonds involved. The relation between bands, bonds, and charge densities has already been given,<sup>10,27,28</sup> the connection to the EFG will be discussed in Sec. VI.

## VI. ORIGIN OF THE EFG AND RELATION TO THE CHARGE DISTRIBUTION

In Sec. IV A the formalism for the computation of the EFG has been described, whose components are expressed in terms of the potential parameters  $V_{LM}$  according to Eq. (5). The latter, defined in Eq. (4), consist of three terms, an integral taken over the atomic sphere (valence EFG) and two more terms called *lattice* EFG. In all three  $\text{YBa}_2\text{Cu}_3\text{O}_x$  calculations the *lattice* EFG contributes at most 8% for the oxygen positions and less than 1% to the total EFG for the copper positions, a situation similar to that found for hcp metals<sup>13</sup> or for  $\text{Cu}_2\text{O}$ .<sup>14</sup> Consequently, for an understanding of the origin of the EFG we can focus on the main component, the *valence* EFG. The ingredients for its calculation are the density coefficients  $\rho_{2M}$  defined in Eq. (3), which originate from two radial wave functions with  $l$  and  $l'$ . The only nonvanishing combinations are of  $p$ - $p$ ,  $d$ - $d$ , or  $s$ - $d$  symmetry, where the last turned out to be very small; therefore, they will be omitted in the following analysis.

### A. The Cu(1) position

The EFG and  $\eta$  on the Cu(1) position (Fig. 1) agree well between our theory and experiment for all three cases of  $\text{YBa}_2\text{Cu}_3\text{O}_7$ ,  $\text{YBa}_2\text{Cu}_3\text{O}_{6.5}$ , and  $\text{YBa}_2\text{Cu}_3\text{O}_6$  (Table I). The  $c$  component  $V_{cc}$  in  $\text{YBa}_2\text{Cu}_3\text{O}_7$  (Table II) is very small, while  $V_{aa}$  and  $V_{bb}$  have similar values with opposite signs leading to an asymmetry parameter  $\eta$  of about 1. Therefore, it is difficult to determine the sign of the EFG unambiguously. In  $\text{YBa}_2\text{Cu}_3\text{O}_{6.5}$  we find  $V_{bb}$  as a principal component which is comparable in magnitude but opposite in sign to  $V_{cc}$ . In  $\text{YBa}_2\text{Cu}_3\text{O}_6$   $\eta$  is 0 due to the tetragonal symmetry, and the EFG is negative and points in the  $c$  direction. We properly describe the increase of the EFG by about 50% from  $\text{YBa}_2\text{Cu}_3\text{O}_7$  to  $\text{YBa}_2\text{Cu}_3\text{O}_6$ , but  $\text{YBa}_2\text{Cu}_3\text{O}_{6.5}$  cannot be obtained by a simple linear interpolation, since the sign changes from positive to negative from  $\text{YBa}_2\text{Cu}_3\text{O}_7$  to  $\text{YBa}_2\text{Cu}_3\text{O}_{6.5}$  for  $V_{bb}$  and from  $\text{YBa}_2\text{Cu}_3\text{O}_{6.5}$  to  $\text{YBa}_2\text{Cu}_3\text{O}_6$  for  $V_{cc}$ . The present results on  $\text{YBa}_2\text{Cu}_3\text{O}_{6.5}$  based on the assumed structure shown in Fig. 2 confirm the interpretation by Lütgemeier,<sup>4</sup> who assigned the observed NMR frequency to a threefold coordinated Cu(1) in oxygen deficient  $\text{YBa}_2\text{Cu}_3\text{O}_x$ .

Figure 4 shows the radial dependence of three types of functions which are needed in the computation of the valence EFG for  $M=0$  and 2. These are described in the following.

(i) The nonspherical charge-density component  $r^2\rho_{2M}(r)$ , which is enhanced for large  $r$ , shows “wiggles” coming from the  $p$  and  $d$  densities originating from the nodal structure of the wave functions (Fig. 6).

(ii) Division by  $r^3$  of the function mentioned in (i) yields the integrand of the first term in Eq. (4) and has

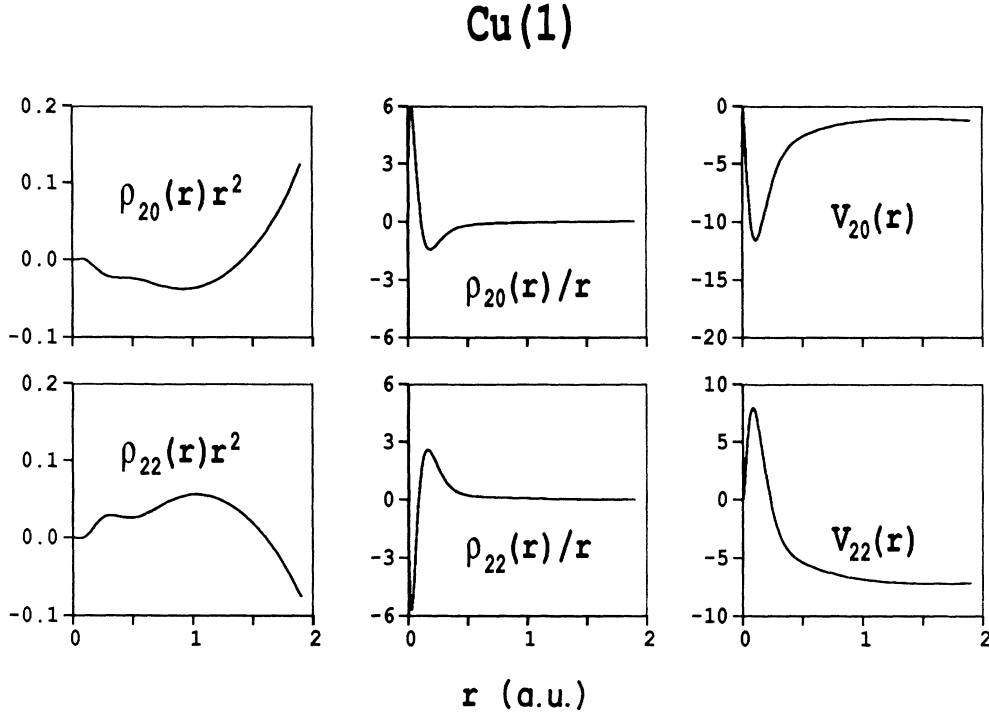


FIG. 4. Inside the Cu(1) sphere the following quantities are shown as function of radius: The nonspherical charge density component  $r^2\rho_{LM}(r)$ ; the EFG integrand  $\rho_{LM}(r)/r$  [first term in Eq. (4)] and the integral up to  $r$ ; the valence EFG contribution from  $V_{LM}(r)$  for  $L=2$  and  $M=0$  (top row) and  $M=2$  (bottom row).

strongly enhanced the oscillations at very short distances. The first sharp peak is caused by the anisotropy of the  $4p$  functions inside the first node, but then the  $3d$  contribution with opposite sign dominates, while even stronger anisotropies at large  $r$  are damped by the  $r^3$  factor.

(iii) The corresponding integral over the second function (multiplied by  $-C_{2M}$ ) is taken up to a radius  $r$  and is labeled  $V_{2M}(r)$ . The large negative  $p$  contribution for  $M=0$  is partly cancelled by the positive  $d$  contribution leading to a small total value for  $V_{20}$ ; a similar cancellation (with opposite signs for  $p$  and  $d$ ) is found for  $V_{22}$ . The fact that both integrals stay rather constant well before the sphere radius is reached, indicates that the valence EFG is determined primarily by contributions relatively close to the nucleus while the *lattice* contribution is extremely small. Since  $V_{22}$  is negative and much larger than  $V_{20}$ , the largest EFG component according to Eq. (5) is  $V_{bb}$ .

### B. The Cu(2) position

In  $\text{YBa}_2\text{Cu}_3\text{O}_7$  we find qualitative agreement with the experimental data, namely that the EFG points into the  $c$  direction while  $V_{aa}$  and  $V_{bb}$  are similar, leading to an  $\eta$  of about 0 (Table II). While the symmetry agrees well, the magnitude of the theoretical EFG is less than half the experimental value for both  $\text{YBa}_2\text{Cu}_3\text{O}_7$  and  $\text{YBa}_2\text{Cu}_3\text{O}_6$  (Table I). Since this seems to be a severe discrepancy, we present a detailed analysis for  $\text{YBa}_2\text{Cu}_3\text{O}_7$ . Figure 5 shows that the EFG at the Cu(2) site originates from the anisotropy of the valence-electron charge distribution,

while contributions from lower-lying semicore states are very small (enlarged 50 times in Fig. 5). The asymmetry of the  $4p$  (the  $p$ - $p$  term to  $\rho_{2M}$ ) and  $3d$  valence electrons (the  $d$ - $d$  term) contribute with  $9.6$  and  $-14.9 \times 10^{-2} \text{ V m}^{-2}$ , respectively, yielding a total EFG of  $-5.6 \times 10^{-2} \text{ V m}^{-2}$ . The  $p$ - $p$  part contributes up to a radius of about the first radial node in the  $3p$  or  $4p$  radial function (Fig. 6), but the  $d$ - $d$  part extends up to about 1 a.u. (Fig. 5) since the  $3d$  function is nodeless.

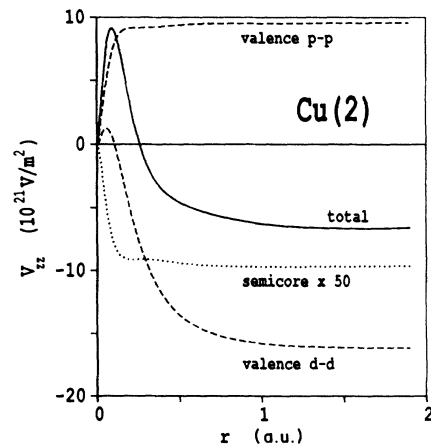


FIG. 5. The EFG contribution  $V_{zz}$  of Cu(2) is shown as a function of radius. A decomposition of the total component into contributions from the Cu  $3p$  semicore states (enlarged 50 times) and the valence  $p$ - $p$  and  $d$ - $d$  parts is displayed.

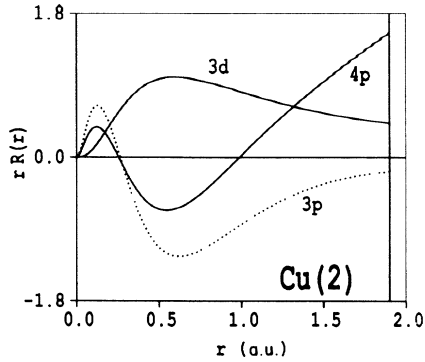


FIG. 6. The radial wave functions (in arbitrary units) of Cu(2) is shown for the 3d and 4p valence states and the 3p semicore states inside the Cu(2) sphere (the energy is taken at the center of the corresponding occupied state).

The EFG can be related to the symmetry-decomposed partial charges which were discussed in Secs. V A and V B (Tables III and IV). In the special case of the Cu(2) position, where  $V_{22}$  is very small, one can split the EFG into contributions from two groups of  $p$  and three groups of  $d$  functions according to the point-group symmetry. In this context it is useful to define an anisotropy count<sup>13,15</sup> in terms of partial charges (labeled by their symmetry)

$$\begin{aligned} \Delta n_p &= \frac{1}{2}(p_x + p_y) - p_z, \\ \Delta n_d &= (d_{xy} + d_{x^2-y^2}) - \frac{1}{2}(d_{xz} + d_{yz}) - d_{z^2}. \end{aligned} \quad (8)$$

The partial charges (Table III), grouped with prefactors and signs according to Eq. (8), contribute with  $n$  to the asymmetry count  $\Delta n$ . These values of  $n$ , the corresponding *valence* EFG contribution, and the ratio  $M_l = V_{zz}^l / n$  are listed in Table V. We have shown<sup>15</sup> that this ratio gives a constant  $M_p$  and  $M_d$  for the  $p$  and  $d$  symmetries, respectively. These factors are proportional to the corresponding  $\langle 1/r^3 \rangle$  expectation value as was demonstrated for  $\text{Cu}_2\text{O}$ .<sup>14</sup> Therefore, the EFG can be obtained directly from the partial charges, provided they are properly grouped and weighted according to Eq. (8) and multiplied by  $M_p$  or  $M_d$ .

This analysis shows the sensitivity of the EFG with respect to charge distributions. Considering that the LDA may not fully account for exchange-correlation effects for rather localized states, such as the Cu 3d, it is sensible to make the following rough estimates.

(i) It is sufficient to transfer only 0.07 electrons from the  $d_{x^2-y^2}$  into the  $d_{z^2}$  orbital to reproduce the experi-

mental EFG. This would lead to  $1.83e$  in  $d_{z^2}$  and  $1.37e$  in  $d_{x^2-y^2}$ , so that the former is practically fully occupied, since its charge is comparable to the other  $d$  symmetries (Table III). By assuming that about  $1.85e$  correspond to full occupation for Cu  $d$  states, we can renormalize the  $d_{x^2-y^2}$  charge to  $1.48e$ , so that about half a hole is found to reside in the Cu(2) orbital with that symmetry, while part of the holes in the  $\text{CuO}_2$  plane belong to O(2) and O(3) in  $p_x$  and  $p_y$  symmetry, respectively, as can be seen from the corresponding partial charges (Table III). Even without this hypothetical charge transfer the character of this  $\sigma$  hole state can be clearly seen as negative  $\Delta\rho$  in Fig. 3.

(ii) The extreme cases, assumed by some many-body models, namely localized Cu 3d electrons with integer occupation numbers (with  $3d^8$  or  $3d^9$ ), can be ruled out since already one missing  $d$  electron of  $x^2-y^2$  symmetry produces an EFG which is about 5 times the experimental value.<sup>15</sup>

### C. The oxygen positions

The contributions to the *valence* EFG are illustrated in Fig. 7 for O(4) as a typical example. Here the  $M=0$  terms are significantly larger than the  $M=2$  terms leading to a small asymmetry parameter  $\eta$ ; consequently, the EFG points in the  $c$  direction. The radial convergence of the sphere contribution  $V_{2M}(r)$  is comparable to Cu (Figs. 4 and 5), although the anion oxygen has diffuse  $2p$  wave functions but the cation Cu has tightly bound 3d functions. This similar radial behavior is consistent with the observed anisotropies which appear in the difference densities (Fig. 3) with maxima and minima found at about the same distance from oxygen or copper, respectively. Since, for oxygen, essentially only the  $p$ - $p$  terms contribute to the EFG, the interpretation is easy: The EFG originates from the anisotropic charge distribution which is shown in the difference density  $\Delta\rho$  (Fig. 3), where the symmetric density has been subtracted. For all oxygen atoms there is a large negative  $\Delta\rho$  in one direction and a smaller positive perpendicular to it. The factor  $1/r^3$  enhances this feature and brings it closer to the nucleus. This function is multiplied by a negative constant according to Eq. (4) and subsequent integration yields the EFG, whose principal component points in the direction of the largest anisotropy, since there is no qualitative change (besides the change of sign) between  $\Delta\rho$  and the final integrand. From this simple argument it is apparent that the main EFG component is positive for all oxygens in  $\text{YBa}_2\text{Cu}_3\text{O}_7$  and points in the  $c$  direction for O(4), but in the  $b$  direction for O(1) and O(3). The largest anisotro-

TABLE V. EFG analysis for Cu(2) in  $\text{YBa}_2\text{Cu}_3\text{O}_7$ : Part of the asymmetry count  $n$  (in electrons), the corresponding *valence* EFG contribution in  $10^{21} \text{ V m}^{-2}$ , and the ratio  $M_l = V_{zz}^l / n$  for  $l = 1, 2$  ( $p$  and  $d$ ).

	$p_x, p_y$	$p_z$	$d_{x^2-y^2}, d_{xy}$	$d_{z^2}$	$d_{xz}, d_{yz}$
$n$	0.072	-0.034	3.293	-1.763	-1.818
$V_{zz}^l$	18.1	-8.5	154.2	-83.0	-86.1
$M_l$	251	250	47	47	47

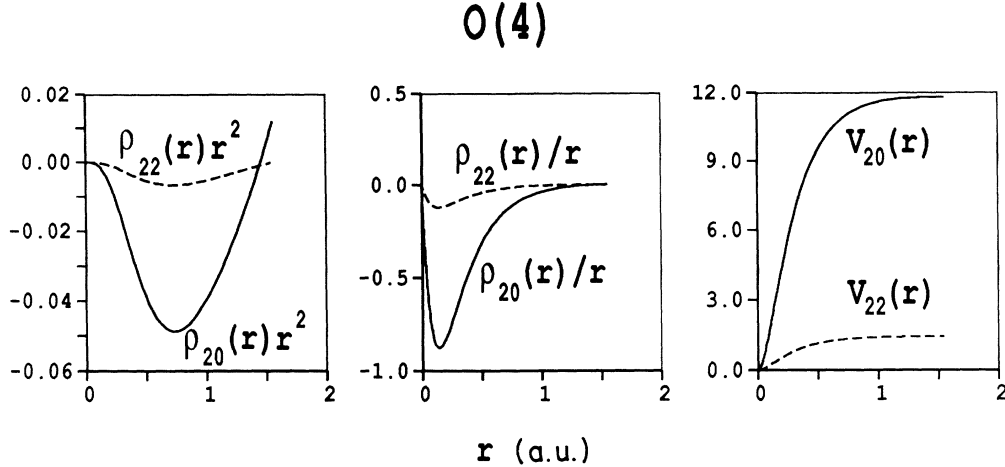


FIG. 7. Inside the O(4) sphere the following quantities are shown as function of radius: The nonspherical charge-density component  $r^2\rho_{LM}(r)$ ; the EFG integrand  $\rho_{LM}(r)/r$  and the valence EFG contribution from  $V_{LM}(r)$  for  $L=2$  and  $M=0$  (solid line) and  $M=2$  (dashed line).

py in  $\Delta\rho$  is found for O(1) yielding the largest EFG among the oxygens. For copper such a simple analysis is not possible, since there is a compensation between  $p$ - $p$  and  $d$ - $d$  contributions.

#### D. The Y position

Although on Y the EFG cannot be measured, its analysis is of fundamental interest, because in this case the Y  $4p$  semicore states dominate over the contributions from the Y  $5p$  (and Y  $4d$ ) valence states as shown in Fig. 8. Consequently, the total EFG requires a proper treatment of the semicore polarization effects, without which neither the signs nor the orientation would be given correctly. Note that in contrast to the situation for Cu (Figs. 4 and 5), or oxygen (Fig. 7), the EFG of Y is converged when the integration over the anisotropic density is taken up to about the first node in the radial  $p$  functions at only a few tenths of an atomic unit, which is far inside the Y sphere radius of 2.74 a.u. (an expanded radial mesh is used in Fig. 8).

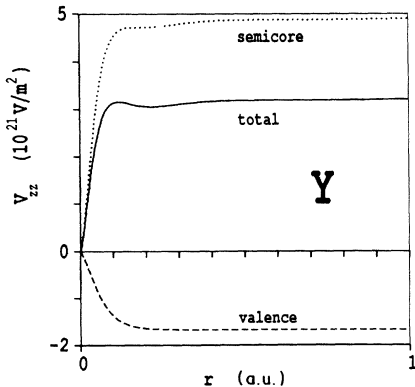


FIG. 8. The EFG contribution  $V_{zz}$  of Y is shown as a function of radius: a decomposition of the total component (solid line) into contributions from the Y  $4p$  semicore (dotted line) and the valence (dashed line) states is displayed.

## VII. DISCUSSION

The traditional interpretation of the principal component of the EFG uses the formula<sup>24</sup>

$$V_{zz} = (1 - \gamma_\infty)V_{zz}^{\text{ext}} + (1 - R)V_{zz}^{\text{local}} \quad (9)$$

which comes about by the following arguments. One starts with an atom or ion in a field of external point charges in a lattice. These external (point) charges generate the field  $V_{zz}^{\text{ext}}$  which must be corrected by a Sternheimer antishielding factor  $\gamma_\infty$  (the latter is often between  $-10$  and  $-80$  and accounts for the perturbing influence of the external potential on the electronic wave functions). This perturbation of the charge distribution creates an additional field at the nucleus. In the case of an asymmetric charge distribution near the nucleus, a local field  $V_{zz}^{\text{local}}$  arises which is affected by a Sternheimer shielding factor  $R$  (in the range  $-0.2 \leq R \leq 0.2$ ) referring to atomic shielding of the EFG. In this model (core) polarization effects in terms of perturbations and (anti) shielding effects are key quantities for an understanding of the origin of the EFG.

The new approach by Blaha *et al.*,<sup>11-16,25</sup> used in the present paper, is a method which allows the computation of EFG's from a given density on a first-principles basis without the need for any Sternheimer factors. All the polarization effects are properly taken care of in the self-consistent band calculation provided the density-functional theory in its LDA form can give a good quality charge density. In this representation the EFG originates from the asymmetry in the charge distribution caused by chemical bonding.

In addition to the LDA, which we want to check, and the convergence of the LAPW calculation, which we have monitored (discussed in Sec. III), small changes in structural parameters could affect the EFG, as was found for example in hcp Be when the  $c/a$  ratio of the lattice parameters is changed.<sup>12</sup> In  $\text{YBa}_2\text{Cu}_3\text{O}_7$  this sensitivity to structural data could be the fractional  $c$  coordinate of the O(4) site (see Fig. 1) or the lattice constants  $a$  and  $b$ .

We have varied these parameters by  $\pm 3\%$  but did not observe dramatic effects on the total EFG's. Although the  $p$  and  $d$  contributions were modified, their changes cancel each other to a large extent; similar to the situation described in Secs. V A and V B in combination with the Figs. 4 and 5.

Our LAPW calculations are non-spin polarized and, thus, for  $\text{YBa}_2\text{Cu}_3\text{O}_6$ , a comparison with experiment is justified only for the Cu(1) position where no magnetic moment is observed, but not for the Cu(2) position which carries a moment. One can argue that even in superconducting  $\text{YBa}_2\text{Cu}_3\text{O}_7$ , magnetic interactions (fluctuations) at the Cu(2) position are present which are omitted in the present calculation and thus could cause the observed discrepancy between our results and experimental EFG's.

It was questioned whether or not the present LDA version can properly describe these highly-correlated systems. A first success of LDA calculations was reported by Cohen *et al.*<sup>35</sup> who studied the equilibrium lattice parameters and the rather delicate phonon frequencies. The present analysis has shown that within the LDA the charge distribution and the electric-field gradients are obtained in close agreement with experimental data. The small change in occupation numbers of  $0.07e$  between

two symmetries of the Cu(2)  $d$  states, which would be needed to make the agreement perfect, indicates that the LDA is rather good, but some intraatomic angular correlations might be underestimated presumably by the implicitly assumed spherical averaging over the exchange-correlation hole. In conclusion, we confirm the picture of the chemical bond in this class of compounds with strong covalent interactions rather than fully localized Cu  $d$  states.

*Note added in proof.* At the International Winter-school on Electronic Properties of High Temperature Superconductors, Lütgemeier<sup>36</sup> presented NQR measurements on  $\text{YBa}_2\text{Cu}_3\text{O}_6$  and  $\text{YBa}_2\text{Cu}_3\text{O}_7$  from which he determined the EFG's at the Ba sites and found good agreement with the values predicted in the present paper.

#### ACKNOWLEDGMENTS

This project was supported by the Fonds zur Förderung der wissenschaftlichen Forschung Project No. P7063P. Some of the calculations were performed on the IBM 3090-400 VF of the computer center of the University of Vienna within the European Academic Supercomputing Initiative (EASI) sponsored by IBM.

- <sup>1</sup>M. Mali, D. Brinkmann, L. Pauli, J. Roos, H. Zimmermann, and J. Hullinger, *Phys. Lett. A* **124**, 112 (1987).
- <sup>2</sup>R. E. Walstedt, W. W. Warren, R. F. Bell, G. F. Brennert, G. P. Espinosa, J. P. Remeika, R. J. Cava, and E. A. Rietmann, *Phys. Rev. B* **36**, 5727 (1987).
- <sup>3</sup>Y. Kitaoka, S. Hiramatsu, T. Kondo, and K. Asyama, *J. Phys. Soc. Jpn.* **57**, 30 (1988).
- <sup>4</sup>H. Lütgemeier, *Physica C* **153-155**, 95 (1988).
- <sup>5</sup>C. H. Pennington, D. J. Durand, D. B. Zax, C. P. Slichter, J. P. Rice, and D. M. Ginsberg, *Phys. Rev. B* **37**, 7944 (1988).
- <sup>6</sup>R. E. Walstedt, W. W. Warren, R. Tycko, R. F. Bell, G. F. Brennert, R. J. Cava, L. Schneemeyer, and J. Waszczak, *Phys. Rev. B* **38**, 9303 (1988).
- <sup>7</sup>C. Coretsopoulos, H. C. Lee, E. Ramli, L. Reven, T. B. Rauchfuss, and E. Oldfield, *Phys. Rev. B* **39**, 781 (1989).
- <sup>8</sup>M. Takigawa, P. C. Hammel, R. H. Heffner, Z. Fisk, K. C. Ott, and J. D. Thompson, *Phys. Rev. Lett.* **63**, 1865 (1989).
- <sup>9</sup>E. Oldfield, Ch. Coretsopoulos, S. Yang, L. Reven, H. C. Lee, J. Shore, O. H. Han, E. Ramli, and D. Hinks, *Phys. Rev. B* **40**, 6832 (1989).
- <sup>10</sup>W. E. Pickett, *Rev. Mod. Phys.* **61**, 433 (1989).
- <sup>11</sup>P. Blaha, K. Schwarz, and P. Herzig, *Phys. Rev. Lett.* **54**, 1192 (1985).
- <sup>12</sup>P. Blaha and K. Schwarz, *J. Phys. F* **17**, 899 (1987).
- <sup>13</sup>P. Blaha, K. Schwarz, and P. H. Dederichs, *Phys. Rev. B* **37**, 2792 (1988).
- <sup>14</sup>P. Blaha and K. Schwarz, *Hyperfine Interact.* **52**, 153 (1989).
- <sup>15</sup>C. Ambrosch-Draxl, P. Blaha, and K. Schwarz, *J. Phys. Condens. Matter* **1**, 4491 (1989).
- <sup>16</sup>C. Ambrosch-Draxl, P. Blaha, and K. Schwarz, *Physica C* **162-164**, 1353 (1989).
- <sup>17</sup>K. T. Park, Ph.D. thesis, University of Tokyo, 1988.
- <sup>18</sup>B. Raveau, C. Michel, M. Hervieu, J. Provost, and F. Studer, in *Earlier and Recent Aspects of Superconductivity*, Vol. 90 of *Springer Series in Solid State Sciences*, edited by J. G. Bednorz and K. A. Müller, (Springer-Verlag, Berlin, 1990), p. 66.
- <sup>19</sup>P. A. Sterne and L. T. Wille, *Physica C* **162-164**, 223 (1989).
- <sup>20</sup>H. Lütgemeier (private communication).
- <sup>21</sup>M. A. Beno, L. Soderholm, D. W. Capone, D. G. Hinks, J. D. Jorgensen, I. K. Schuller, C. U. Segre, K. Zhang, and J. D. Grace, *Appl. Phys. Lett.* **51**, 57 (1987).
- <sup>22</sup>A. W. Hewat, J. J. Capponi, C. Chaillout, M. Marezio, and E. A. Hewat, *Solid State Commun.* **64**, 301 (1987).
- <sup>23</sup>P. Blaha, K. Schwarz, P. Sorantin, and S. B. Trickey, *Comput. Phys. Commun.* (to be published).
- <sup>24</sup>E. N. Kaufman and R. J. Vianden, *Rev. Mod. Phys.* **51**, 161 (1979).
- <sup>25</sup>P. Blaha, P. Sorantin, C. Ambrosch, and K. Schwarz, *Hyperfine Interact.* **51**, 917 (1989).
- <sup>26</sup>M. Weinert, *J. Math. Phys.* **22**, 2433 (1981).
- <sup>27</sup>H. Krakauer, W. E. Pickett, and R. E. Cohen, *J. Supercon.* **1**, 111 (1988).
- <sup>28</sup>J. Yu, S. Massidda, A. J. Freeman, and D. D. Koelling, *Phys. Lett. A* **122**, 203 (1987).
- <sup>29</sup>R. M. Sternheimer, *Z. Naturforsch.* **41a**, 24 (1986).
- <sup>30</sup>M. J. Stevenson and C. H. Townes, *Phys. Rev.* **107**, 635 (1957).
- <sup>31</sup>P. Sorantin, Ph.D. thesis, Technical University Vienna, 1990.
- <sup>32</sup>A. Bianconi, A. C. Castellano, M. De Santis, P. Rudolf, P. Lagarde, A. M. Flank, and A. Marcelli, *Solid State Commun.* **63**, 1009 (1987).
- <sup>33</sup>N. Nücker, H. Romberg, X. X. Xi, J. Fink, B. Gegenheimer, and Z. X. Zhao, *Phys. Rev. B* **39**, 6619 (1989).
- <sup>34</sup>H. Yasuoka, T. Shimizu, Y. Ueda, and K. Kosuge, *J. Phys. Soc. Jpn.* **57**, 2659 (1988).
- <sup>35</sup>R. E. Cohen, W. E. Pickett, and H. Krakauer, *Phys. Rev. Lett.* **62**, 831 (1989).
- <sup>36</sup>H. Lütgemeier, in *Electronic Properties of High- $T_c$  Superconductors and Related Compounds*, Springer Series in Solid State Sciences, Proceedings of the International Winterschool on Electronic Properties of High Temperature Superconductors, Kirchberg, Austria, 1990, edited by H. Kuzmany, M. Mehringer, and J. Fink (Springer-Verlag, Berlin, in press).

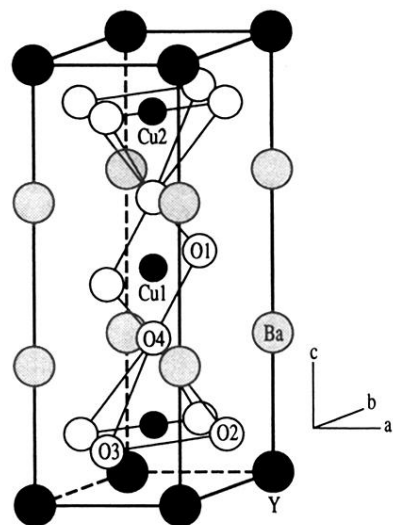


FIG. 1. Unit cell of  $\text{YBa}_2\text{Cu}_3\text{O}_7$ , with standard labeling of the atoms.

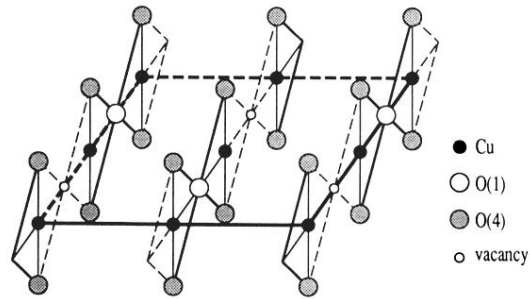


FIG. 2. In  $\text{YBa}_2\text{Cu}_3\text{O}_{6.5}$  half of the O(1) atoms (see Fig. 1) are missing. Here an ordered defect structure is assumed in which Cu(1) is threefold coordinated and the oxygen vacancies alternate in neighboring Cu(1)-O(1) chains in a certain pattern. In addition, the O(4) atoms above and below the Cu(1)-O(1) plane are shown. The other atoms [Cu(2), O(2), O(3), Y, and Ba] have the corresponding positions as in  $\text{YBa}_2\text{Cu}_3\text{O}_7$  (see Sec. II).